

Beyond Ginibre statistics in open Floquet chaotic systems with localized leaks

Edson M. Signor,¹ Miguel A. Prado Reynoso,¹ Bidhi Vijaywargia,¹ S. D. Prado,² and Lea F. Santos¹

¹*Department of Physics, University of Connecticut, Storrs, Connecticut 06269, USA.*

²*Instituto de Física, Universidade Federal do Rio Grande do Sul, Porto Alegre CP15051, Brazil.*

We show that the spectral properties of driven quantum systems with a classically chaotic counterpart and spatially localized openness, such as optical or microwave billiards with leaks, deviate from predictions of Ginibre ensembles. Our analysis focuses on the leaky quantum standard map (QSM) of the kicked rotor. We compare its complex resonance spectrum with both Ginibre and truncated circular orthogonal ensembles (TCOEs). We find that the long-lived resonances follow TCOE statistics, reproducing the density of states and level spacing correlations, but depart from Ginibre predictions. Short-lived resonances, however, do not show a clear correspondence with either random-matrix ensemble. We also demonstrate that increasing the leak size takes the density of states of the TCOE toward the Ginibre limit, yet their spectral correlations remain distinct.

I. INTRODUCTION

Quantum chaos refers to properties of the spectra and eigenstates of quantum systems that reflect the chaotic dynamics of their classical counterparts. In particular, spectral correlations that follow the predictions of random matrix theory serve as signatures of underlying classical chaos. For isolated quantum systems described by time-independent Hamiltonians, chaos implies spectral fluctuations that obey Wigner-Dyson statistics, while the correlations of the quasienergies of periodically driven (Floquet) systems are consistent with Dyson's circular ensembles [1–5]. When a quantum system is opened to an external environment, its dynamics becomes non-unitary, the spectrum becomes complex [6–22] and the eigenstates are no longer orthonormal [23–25], motivating extensions of quantum chaos diagnostics to the non-Hermitian domain.

According to the Grobe-Haake-Sommer conjecture [6–17], first introduced in the context of the periodically kicked top with damping, the spectral statistics of open quantum systems that are chaotic in the classical limit follow those of Ginibre ensembles [26–28], characterized by a uniform distribution of the eigenvalues over the complex plane and cubic level repulsion. However, subsequent refinements and tests of this conjecture have revealed a broader picture. Ginibre-like level repulsion is not an exclusive signature of classical chaos, as it can also arise in non-Hermitian spectra without an underlying classical chaotic dynamics [29–32]. In parallel, and closer in spirit to the present study, additional non-Hermitian universality classes have been identified [10, 33], giving rise to spacing distributions that differ from the Ginibre case [10].

In this work, we investigate the spectral properties of a periodically driven quantum system with a spatially localized opening, analogous to a leak in optical or microwave billiards [34–37]. Our central question is whether Ginibre universality persists under such conditions. We show that it does not; non-Hermiticity introduced by localized openness leads to deviations from Ginibre statistics.

Our analysis focuses on the spectrum of the strongly chaotic quantum standard map (QSM), which corresponds to the one-period Floquet operator of the quantum kicked rotor [38]. Openness is introduced via a localized leak, modeled by truncating the unitary Floquet propagator, that is, by setting to zero the columns of the propagator associated with the position of the opening [39]. The resulting truncated Floquet operator is non-unitary and produces a spectrum of complex resonances. This formulation is naturally related to the truncated circular orthogonal ensemble (TCOE) of random matrix theory [40–43], where a unitary matrix is partially truncated to emulate openness.

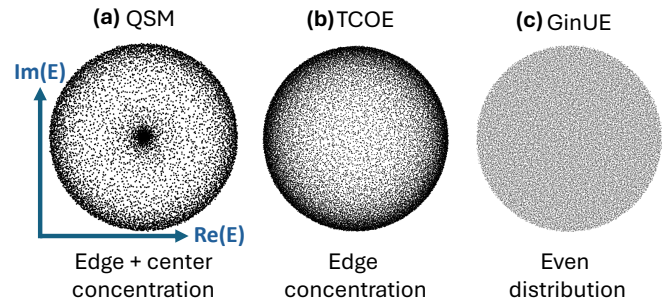


FIG. 1. Sketch of the distributions of the eigenvalues over the complex plane for the (a) leaky quantum standard map, (b) truncated circular orthogonal ensemble, and (c) Ginibre unitary ensemble.

We compare the spectrum of the leaky QSM with those of the Ginibre unitary ensemble (GinUE) and the TCOE. A summary of the results is sketched in Fig. 1. While the eigenvalues of the Ginibre ensemble are uniformly distributed over the complex plane [Fig. 1(c)], both the TCOE [Fig. 1(b)] and the leaky QSM [Fig. 1(a)] display a clear concentration of long-lived resonances near the unit circle. This similarity between the leaky QSM and TCOE breaks down for short-lived resonances, as the QSM spectrum exhibits an additional clustering of resonances near the origin, which is absent in the TCOE. These observations lead to the following conclusions for open systems with a leak of moderate size:

- *Long-lived resonances:* For this part of the spectrum, the density of states and spectral correlations of the leaky QSM exhibit excellent agreement with TCOE predictions, but deviate from the GinUE.

- *Short-lived resonances:* This part of the spectrum of the leaky QSM shows no clear correspondence with either the TCOE or the GinUE. These short-lived resonances originate from non-ergodic Floquet states that localize near the leak and therefore retain system-specific structure. They have been studied in [44, 45].

Furthermore, motivated by the studies in [40], we investigate the spectral properties of the TCOE as the degree of truncation increases, that is, as a larger fraction of columns is set to zero. As anticipated in Ref. [40], we find that the density of states gradually approaches that of the GinUE. However, we do not observe convergence of the spectral correlations of the TCOE to those of Ginibre.

The paper is organized as follows. Section II reviews the classical and quantum standard map and describes the model with a leak. In Sec. III, we compare the density of states and spectral correlations of the leaky QSM with those of the TCOE and GinUE, revealing close agreement with the TCOE but clear deviations from Ginibre statistics. Section IV examines how increasing the size of the leak takes the TCOE density of states toward the Ginibre limit, while the spectral correlations remain distinct. Our conclusions are presented in Sec. V.

II. CLASSICAL AND QUANTUM STANDARD MAP WITH LEAKAGE

We begin by reviewing the closed standard map in the classical and quantum domains, followed by a description of the system when a leak is introduced.

A. Closed standard map

A classical kicked rotor consists of a rotor that receives periodic instantaneous “kicks” and moves freely between them. Its Hamiltonian is given by

$$H(q, p) = \frac{p^2}{2} - \frac{K}{4\pi^2} \cos(2\pi q) \sum_{n=-\infty}^{\infty} \delta(t - n), \quad (1)$$

where q is the angular position, p is the conjugate momentum, K is the kick strength that controls the nonlinearity of the system, and the kicking period is set to unity. Integrating Hamilton’s equations over one period, from just after kick n to just after kick $n+1$, we can construct the discrete-time standard map (Chirikov map) [46, 47],

$$\begin{aligned} q_{n+1} &= q_n + p_n \pmod{1} \\ p_{n+1} &= p_n - \frac{K}{2\pi} \sin(2\pi q_{n+1}) \pmod{1}, \end{aligned} \quad (2)$$

where both canonical variables (q, p) are taken modulo 1, confining the motion to a toroidal phase space \mathbb{T}^2 with dimensionless coordinates $q, p \in [0, 1]$.

The parameter K governs the transition from regular to chaotic motion. For $K = 0$, the dynamics is integrable. As K increases, the system enters a mixed phase-space regime, characterized by the coexistence of chaotic seas and stable islands, as illustrated in Fig. 2(a) for $K = 1.5$. For sufficiently large K , the stable islands are destroyed and the dynamics become fully chaotic, as shown in Fig. 2(b) for $K = 10$. This large value of K is used for all results presented in this work.

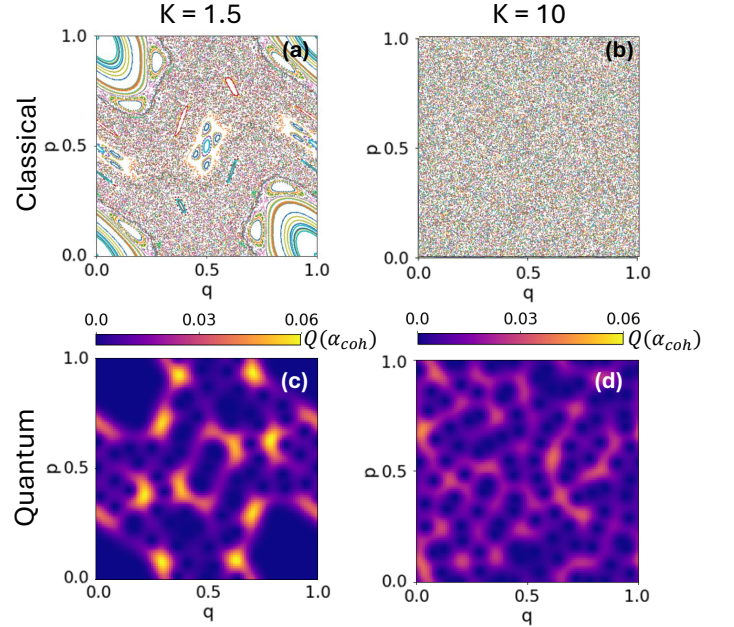


FIG. 2. Classical-quantum correspondence of the closed standard map for (a),(c) mixed phase-space regime at $K = 1.5$ and (b),(d) fully chaotic regime at $K = 10$. (a)-(b) Classical phase-space landscapes and (c)-(d) Husimi Q-functions of selected eigenstates.

The quantum kicked rotor is obtained by quantizing the classical Hamiltonian in Eq. (1). Because the classical phase space of the standard map is compact with unit area, quantization restricts the system to a finite Hilbert space of dimension $N = 1/(2\pi\hbar)$, where each one of the N quantum states occupies a minimal phase-space area of size $2\pi\hbar$ with \hbar being the effective Planck constant [48]. The canonical commutation relation $[\hat{q}, \hat{p}] = i\hbar$ is enforced, and the toroidal phase space leads to periodic boundary conditions in both position and momentum. As a result, both variables become discrete, taking values on the uniform grid,

$$q_n = \frac{n + \varphi}{N}, \quad p_m = \frac{m}{N}, \quad n, m = 1, \dots, N,$$

where φ specifies the boundary-condition phase associated with torus quantization. Specifically, the quantum standard map requires the wavefunctions to satisfy

$\psi(q+1) = e^{2\pi i \varphi} \psi(q)$. In our calculations, we fix $\varphi = 0.25$ to avoid symmetries associated with periodic boundary conditions ($\varphi = 0$) [38, 49].

The system evolves under the Floquet operator of the quantum standard map (QSM), which for a unit period takes the form

$$\hat{U} = \hat{U}_{\text{kick}} \hat{U}_{\text{free}} = \exp\left[\frac{iK}{4\pi^2\hbar} \cos(2\pi\hat{q})\right] \exp\left[-\frac{i}{\hbar} \frac{\hat{p}^2}{2}\right], \quad (3)$$

where \hat{U}_{kick} represents the instantaneous kick and \hat{U}_{free} the free evolution between two kicks [50]. On the discrete torus, in the position representation, these operators are given by

$$\langle q_n | \hat{U}_{\text{kick}} | q_{n'} \rangle = \exp\left\{i \frac{KN}{2\pi} \cos\left[\frac{2\pi}{N}(n + \varphi)\right]\right\} \delta_{n,n'} \quad (4)$$

$$\langle q_n | \hat{U}_{\text{free}} | q_{n'} \rangle = \sum_m \langle q_n | p_m \rangle \exp\left[-i \frac{\pi m^2}{N}\right] \langle p_m | q_{n'} \rangle. \quad (5)$$

Using the discrete Fourier overlap,

$$\langle q_n | p_m \rangle = \frac{1}{\sqrt{N}} \exp\left[\frac{2\pi i}{N} m(n + \varphi)\right], \quad (6)$$

and the quadratic Gaussian sum,

$$\frac{1}{N} \sum_{m=0}^{N-1} e^{-i \frac{\pi}{N} m^2 + i \frac{2\pi}{N} m(n - n')} = \sqrt{\frac{i}{N}} e^{i \frac{\pi}{N} (n - n')^2}, \quad (7)$$

we obtain

$$U_{n,n'} = \sqrt{\frac{i}{N}} \exp\left\{\frac{i\pi}{N}(n - n')^2 + \frac{iNK}{2\pi} \cos\left[\frac{2\pi}{N}(n + \varphi)\right]\right\}. \quad (8)$$

The spectral decomposition of the Floquet operator,

$$\hat{U} | \phi_\mu \rangle = e^{i\vartheta_\mu} | \phi_\mu \rangle, \quad (9)$$

yields the quasienergies (or eigenangles) $\vartheta_\mu \in [-\pi, \pi]$ and the corresponding Floquet eigenstates $|\phi_\mu\rangle$. The phase-space structures of these eigenstates exhibit a clear correspondence with the underlying classical dynamics. This correspondence becomes evident when the eigenstates are represented through their Husimi Q -functions,

$$Q_\mu(\alpha_{\text{coh}}) = \frac{N}{2\pi} |\langle \alpha_{\text{coh}} | \phi_\mu \rangle|^2, \quad (10)$$

where $|\alpha_{\text{coh}}\rangle$ denotes a coherent state centered at the phase-space point $(q, p) \in \mathbb{T}^2$ [51–54].

Figure 2 illustrates this quantum-classical correspondence. For $K = 1.5$ [Fig. 2(c)], the Husimi distribution of a typical eigenstate is concentrated in the regular islands, reflecting the mixed phase-space structure of the classical dynamics. For $K = 10$ [Fig. 2(d)], the Husimi function becomes delocalized over the entire chaotic sea, consistent with the ergodic character of the underlying classical motion [53].

B. Open standard map with a single leak

We open the system by introducing a leak of width Δq centered at position \bar{q}_L . In phase space, this leak corresponds to a vertical strip parallel to the momentum axis, as shown with a shaded rectangle centered at $\bar{q}_L = 0.2$ in Figs. 3(a,c). Classically, the dynamics follow those of the closed map until a trajectory enters the leak region, $q \in [\bar{q}_L - \Delta q/2, \bar{q}_L + \Delta q/2]$, at which point the trajectory is terminated, representing the escape of the particle through the opening [34, 44].

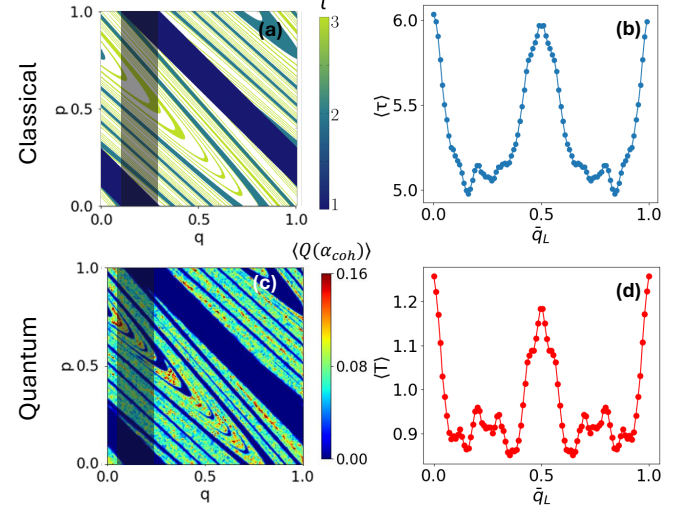


FIG. 3. Open (a)-(b) classical and (c)-(d) quantum standard map with leakage; $\Delta q = 0.2$, $K = 10$, and, for the quantum case, $N = 10^4$. (a) Map of the classical dwell time τ for a slit (shaded area) centered at $\bar{q}_L = 0.2$. Dark blue indicates trajectories that escape after $\tau = 1$ iteration; blue for $\tau = 2$; green for $\tau = 3$; and white corresponds to long-lived trajectories ($\tau > 3$). (b) Classical dwell time averaged over the phase space, $\langle \tau \rangle$, as a function of the slit position \bar{q}_L . (c) Husimi Q -function averaged over the 20 longest-lived eigenstates. The probability density follows the classical dwell-time landscape: it is suppressed in regions where the classical trajectories escape rapidly and enhanced in regions associated with long classical dwell times. (d) Quantum dwell time averaged over all eigenstates, $\langle T \rangle$, as a function of the slit position: its behavior mirrors the dependence of the classical dwell time on \bar{q}_L .

The quantum counterpart of the classical open standard map is described by a non-unitary Floquet operator denoted by \tilde{U} . The opening is modeled by a projection operator $\tilde{\Pi}$ that eliminates probability amplitude in the leaked region of phase space [39]. The resulting open-system propagator is therefore given by

$$\tilde{U} = \hat{U} \tilde{\Pi}. \quad (11)$$

Since the leak corresponds to a vertical strip parallel to the momentum axis in phase space, the projection operator is diagonal in the position basis, and its diagonal

elements are

$$\Pi_{nn} = \begin{cases} 0, & \text{if } n \in \text{leak region,} \\ 1, & \text{otherwise.} \end{cases}$$

Consequently, \tilde{U} coincides with the closed-system propagator except for the columns corresponding to the leak positions which are set to zero. These positions are given by the integer indices

$$n = Nq \in \left\lfloor N\left(\bar{q}_L - \frac{\Delta q}{2}, \bar{q}_L + \frac{\Delta q}{2}\right) \right\rfloor, \quad (12)$$

where $\lfloor x \rfloor$ indicates the integer part of x .

In the spectrum of the operator \tilde{U} ,

$$\tilde{U}|\phi_\mu^R\rangle = \lambda_\mu|\phi_\mu^R\rangle = e^{i\varepsilon_\mu}|\phi_\mu^R\rangle, \quad (13)$$

the complex Floquet eigenvalues (Floquet resonances) λ_μ no longer lie on the unit circle, leading to $|\lambda_\mu| \leq 1$, as evident in Fig. 1(a), and the quasienergies ε_μ are now complex,

$$\varepsilon_\mu = \vartheta_\mu + \frac{i}{2}\Gamma_\mu, \quad (14)$$

where $\vartheta_\mu \in [-\pi, \pi)$ and $\Gamma_\mu > 0$ gives the decay rate of each resonance, defining the quantum dwell time

$$T_\mu = \frac{1}{\Gamma_\mu}. \quad (15)$$

The right and left eigenstates of \tilde{U} , denoted $|\phi_\mu^R\rangle$ and $|\phi_\mu^L\rangle$, form a biorthogonal set, where $|\phi_\mu^R\rangle$ describes forward evolution and $|\phi_\mu^L\rangle$ corresponds to backward propagation [44, 55].

Figure 3(a) shows that the dwell time for trajectories initialized across the phase space vary significantly. Dark blue corresponds to trajectories that escape after a single iteration ($\tau = 1$); lighter blue to those escaping after two iterations ($\tau = 2$); green for three ($\tau = 3$); and white indicates long-lived trajectories ($\tau > 3$).

Figure 3(b) highlights the effects of stickiness, as we now explain. As shown in Ref. [56], even in the strongly chaotic regime, the standard map exhibits stickiness – inhomogeneous structures in phase space, where chaotic trajectories can become temporarily trapped before eventually escaping. These structures are barely perceptible in the closed system due to rapid mixing, but they are revealed once a leak is introduced. This is because the trajectories are terminated upon reaching the leak, which interrupts the mixing process and effectively “freezes” the short-time imprint of these inhomogeneities, making them visible. This behavior is confirmed in Fig. 3(b), which shows the average classical dwell time as a function of the leak position. The dwell time is systematically larger when the leak covers portions of phase space with enhanced stickiness.

Quantum dynamics mirrors the classical behavior. In Fig. 3(c), the Husimi Q-function averaged over long-lived resonances shows enhanced probability density (red dots) in the same regions where the classical dwell time is largest. The quantum-classical correspondence is further demonstrated in Fig. 3(d), where the average quantum dwell time shows the same dependence on the position of the leak as the average classical dwell time in Fig. 3(b). The leak acts as a probe that exposes the fine structure of the classical chaotic phase space, revealing the influence of stickiness on both classical and quantum dynamics.

III. SPECTRAL PROPERTIES OF THE LEAKY QUANTUM STANDARD MAP

To characterize the spectral properties of the leaky QSM, we compare its density of states and spectral correlations with those of the truncated circular orthogonal ensemble (TCOE) and the Ginibre unitary ensemble (GinUE). In all three cases, the matrices are non-Hermitian and have complex entries.

Truncated circular orthogonal ensemble: Because the standard map originates from a time-reversal invariant Hamiltonian, the spectrum of its unitary Floquet propagator \hat{U} is expected to follow the circular orthogonal ensemble (COE) statistics. Therefore, when a localized leak is introduced, the corresponding non-unitary operator of the open QSM, \tilde{U} , is naturally compared with the TCOE. In this ensemble, $N \times N$ matrices are drawn from the COE, and n_L columns have their elements set to zero. The truncation ratio n_L/N directly corresponds to the leak size Δq in the open map,

$$\Delta q = \frac{n_L}{N}. \quad (16)$$

In the non-Hermitian setting of the leaky QSM and the TCOE, the orthogonal symmetry present in the closed system is no longer preserved.

Ginibre unitary ensemble: The GinUE consists of $N \times N$ matrices with independent complex Gaussian entries [26, 57], defined as

$$G_{ij} = \frac{\mathcal{N}(0, 1) + i\mathcal{N}(0, 1)}{\sqrt{2N}}. \quad (17)$$

We choose this ensemble over the Ginibre orthogonal ensemble, because both ensembles share the same density of states [8, 10] and the same nearest-neighbor eigenvalue-spacing statistics in the bulk [10], yet only the GinUE has complex elements.

Normalized spectrum of TCOE and leaky QSM: To enable consistent comparison across different leakage strengths, we normalize each spectrum $\{\lambda_\mu\}$ of the leaky QSM and of the TCOE by its maximal eigenvalue $\lambda_{\max} = \max(\{\lambda_\mu\})$. This rescaling removes differences in the overall decay scale while preserving the spectral structure.

Exclusion of the short-lived states in the leaky QSM: When comparing the spectrum of a physical system with random-matrix ensembles, it is important to exclude system-specific features that obscure universal behavior. In the leaky QSM, such nonuniversal contributions arise from fast-decaying states. The structures of these states are correlated with the location of the leak. Rather than spreading ergodically over phase space, they stem from non-ergodic Floquet states of the closed system that concentrate near the region where the leak is introduced. These short-lived resonances produce the dense cluster of quasienergies near the origin of the complex plane in Fig. 1(a). They have been extensively studied in previous works [44, 55, 58, 59], but are excluded here, as our analysis focuses on universal spectral properties.

To determine the exclusion threshold, we use the smallest absolute values of the Floquet eigenvalues $|\lambda|$ obtained from the TCOE with the same leak size Δq as the open QSM. Unlike the physical quantum map [Fig. 3(d)], the dwell times of the TCOE are independent of the leak position by construction. Hence, the minimal $|\lambda|$ values of the TCOE provide a natural benchmark for decay rates originating purely from stochastic openness, free of dynamical correlations.

Following this criterion, we discard eigenvalues with $|\lambda| < 10^{-1}$ (corresponding to dwell times $\tau < 0.22$), retaining only the subset of resonances expected to display universal chaotic statistics. This filtering process significantly increases the computational cost of the spectral analysis. For a leak size of $\Delta q = 0.2$, roughly half of the spectrum must be excluded, and the fraction grows rapidly as the leak becomes larger. To compensate for the reduced number of usable eigenvalues, we construct an ensemble of QSM spectra by varying the kick strength within the range $9.99 < K < 10.01$, using increments that ensure a total data set of at least 10^5 eigenvalues.

A. Density of states

The density of states is denoted by

$$R_1(\lambda) = \sum_{\mu} \delta(\lambda - \lambda_{\mu}). \quad (18)$$

For the GinUE, where the eigenvalues form a uniform two-dimensional distribution over the complex plane in the large- N limit, the corresponding single-point spectral density is

$$R_1(\lambda) = \frac{1}{\pi}, \quad (19)$$

known as the Ginibre circular law.

Rather than visualizing the full two-dimensional density of states in a three-dimensional plot, we compute $R_1(\lambda)$ from the complex eigenvalues and plot it as a function of their modulus $|\lambda|$. Since different eigenvalues may have the same absolute value, multiple points can fall into the same $|\lambda|$ bin. We use bins of width 10^{-2} .

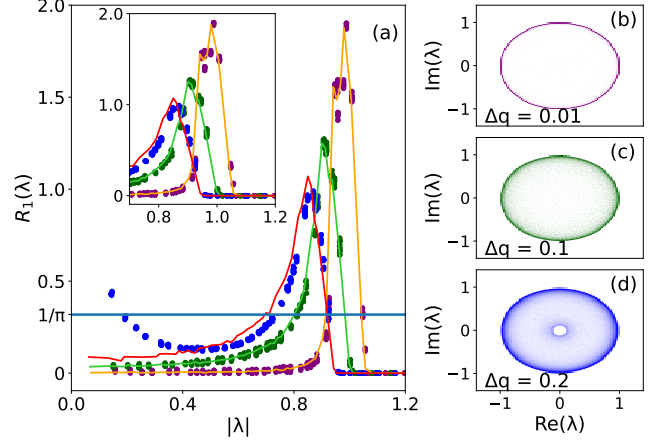


FIG. 4. (a) Averaged density of states $R_1(\lambda)$ of the complex eigenvalues λ of the leaky QSM (circles), TCOE (solid curves), and GinUE (horizontal line at $1/\pi$) plotted as a function of the modulus $|\lambda|$. The leak is centered at $\bar{q}_L = 0.2$ and three slit sizes are shown: $\Delta q = 0.2$ (blue circles and red line), $\Delta q = 0.1$ (green circles and light-green line), and $\Delta q = 0.01$ (purple circles and orange line). The agreement between the leaky QSM and the TCOE progressively extends to the region of low $|\lambda|$ as Δq decreases. The inset highlights the region of long-lived resonances, where there is excellent agreement between QSM and TCOE for all slit sizes. (b)-(d): Rescaled two-dimensional density of states of the leaky QSM for increasing slit size from (b) to (d). The white hole around the origin, clearly visible in (d), corresponds to the excluded short-lived resonances, as described in the text. For each value of Δq , multiple ensemble realizations are considered to ensure a total of at least 10^5 eigenvalues. The QSM ensemble is generated with $9.99 < K < 10.01$.

Figure 4(a) compares the density of states of the leaky QSM with those of the TCOE and the GinUE (shown as the flat reference line at $1/\pi$). The circles correspond to the leaky-QSM data and, as noted above, more than one circle may appear at a given $|\lambda|$. The solid curves represent the TCOE results and are obtained by averaging over all points that fall into each bin.

For the slit of size $\Delta q = 0.2$ in Fig. 4(a), the QSM data are shown as blue circles and the TCOE as a red curve. Two main features emerge: (i) a clear deviation from the uniform GinUE prediction, and (ii) strong agreement with the TCOE for slow-decaying resonances, that is, eigenvalues with large $|\lambda|$. This agreement gradually deteriorates as $|\lambda|$ decreases, despite the prior removal of the resonances with dwell times $\tau < 0.22$.

Contrary to the GinUE, both the leaky QSM and the TCOE exhibit a concentration of long-lived resonances seen as an accumulation of eigenvalues near the unit circle in Fig. 1(a) and Fig. 4(d) for the leaky QSM and similarly in Fig. 1(b) and Fig. 6(b) for the TCOE. This behavior appears as a peak in Fig. 4(a). In the QSM, these long-lived resonances correspond to classical trajectories that avoid the leak for many iterations, and therefore explore the phase space nearly ergodically. Because they

remain effectively uncorrelated with the leak, their spectral properties reproduce those of the TCOE. In contrast, the surviving short-lived resonances of the open QSM retain some degree of correlation with the leak, leading to deviations from TCOE statistics.

As the size of the leak is reduced in Fig. 4(a), the agreement between the density of states of the leaky QSM (circles) and the TCOE (solid lines) progressively extends into the region of lower $|\lambda|$. This trend is clearly visible when comparing the results for $\Delta q = 0.2$ (blue circles and red curve) with those for $\Delta q = 0.1$ (green circles and light-green curve) and $\Delta q = 0.01$ (purple circles and orange curve). As Δq increases, the peak of the spectral distribution shifts toward $|\lambda| \rightarrow 1$, becoming more pronounced near the unit circle, while the density decreases at small $|\lambda|$.

This shift reflects the gradual approach to the closed system, as illustrated by the two-dimensional density of states of the leaky QSM shown in Figs. 4(b)-(d). As the leak decreases from the bottom panel (d) to the top panel (b), the eigenvalues migrate away from the origin and further accumulate near the unit circle. In the limit $\Delta q \rightarrow 0$, the effect of leakage becomes negligible and the spectrum approaches that of the closed QSM, recovering COE statistics.

All results in Fig. 4 correspond to a leak centered at $\bar{q}_L = 0.2$. If the leak is instead placed at $\bar{q}_L = 0.5$ (data not shown), the peak of the density of states $R_1(\lambda)$ shifts toward larger values of $|\lambda|$, indicating a higher proportion of long-lived resonances. This behavior is consistent with the dependence of the quantum dwell time on \bar{q}_L presented in Fig. 3(d), where the influence of stickiness is evident. As demonstrated in Ref. [56], the region around $\bar{q}_L = 0.2$ exhibits stronger sticky structures than the region near $\bar{q}_L = 0.5$. When the leak covers a sticky region (as at $\bar{q}_L = 0.2$), classical trajectories are more efficiently removed, resulting in a larger fraction of short-lived resonances. Conversely, placing the leak in a less sticky region (such as $\bar{q}_L = 0.5$) preserves more long-lived resonances, shifting the spectral weight closer to the unit circle. This case deviates more from the TCOE than having the leak at $\bar{q}_L = 0.2$.

B. Spectral correlations

Two commonly adopted strategies to characterize short-range spectral correlations are the nearest-neighbor eigenvalue spacing distribution and the ratio of consecutive eigenvalue spacings. Both are used here.

1. Nearest-neighbor eigenvalue spacing distribution

Since the eigenvalues λ_μ of the non-Hermitian matrices studied here lie in the complex plane, the nearest-neighbor eigenvalue spacing is defined as the minimal

Euclidean distance,

$$s_\mu = |\lambda_\mu - \lambda_\mu^{\text{NN}}|, \quad (20)$$

between λ_μ and the eigenvalue λ_μ^{NN} that is its nearest neighbor in the complex plane.

Unfolding of complex spectra: As in Hermitian random-matrix theory, unfolding is necessary to separate system-specific spectral features from universal fluctuations. For a spectrum with density of states $R_1(\lambda)$, this decomposition reads

$$R_1(\lambda) = \bar{R}_1(\lambda) + \delta R_1(\lambda), \quad (21)$$

where $\bar{R}_1(\lambda)$ captures the smooth, nonuniversal part of the density of states, and $\delta R_1(\lambda)$ encodes the universal correlations of interest.

Several approaches have been proposed for estimating $\bar{R}_1(\lambda)$ [8, 60, 61]. In the case of locally isotropic spectra, \bar{R}_1 can be approximated by a sum of Gaussians [8]. If the eigenvalue distribution depends only on the radius, not on the angle, one can fit the radial profile or use a theoretical closed form [60, 61].

Here, we employ the well-established local rescaling method described in [4, 6, 62], which is accurate and computationally efficient. The local mean density is estimated as

$$\bar{R}_1(\lambda_\mu) = \frac{k}{\pi d_{k,\mu}^2}, \quad (22)$$

where k is an integer chosen in the range $1 \ll k \ll N$ and $d_{k,\mu}$ is the distance from λ_μ to its k -th nearest neighbor eigenvalue in the complex plane. In our calculations, we choose $k = 30$. This procedure amounts to computing the area of a disk of radius $d_{k,\mu}$ centered at λ_μ and then obtaining the unfolded spacings through the local rescaling [63],

$$\tilde{s}_\mu = s_\mu \sqrt{\bar{R}_1(\lambda_\mu)}. \quad (23)$$

Boundary effects vanish in the limit $N \rightarrow \infty$ with $k/N \rightarrow 0$.

The unfolded spacing distribution $p(\tilde{s})$ is normalized as

$$\int_0^\infty p(\tilde{s}) d\tilde{s} = \int_0^\infty \tilde{s} p(\tilde{s}) d\tilde{s} = 1. \quad (24)$$

According to the Grobe–Haake–Sommer conjecture [6], open quantum systems with classically chaotic dynamics exhibit the same nearest-neighbor eigenvalue spacing distribution as the GinUE, which is given by

$$p_{\text{GinUE}}(s) = C \tilde{p}(Cs), \quad (25)$$

with kernel

$$\tilde{p}(s) = \sum_{j=1}^{\infty} \frac{2s^{2j+1} e^{-s^2}}{\Gamma(j+1, s^2)} \prod_{j=1}^{\infty} \frac{\Gamma(j+1, s^2)}{\Gamma(j+1)}, \quad (26)$$

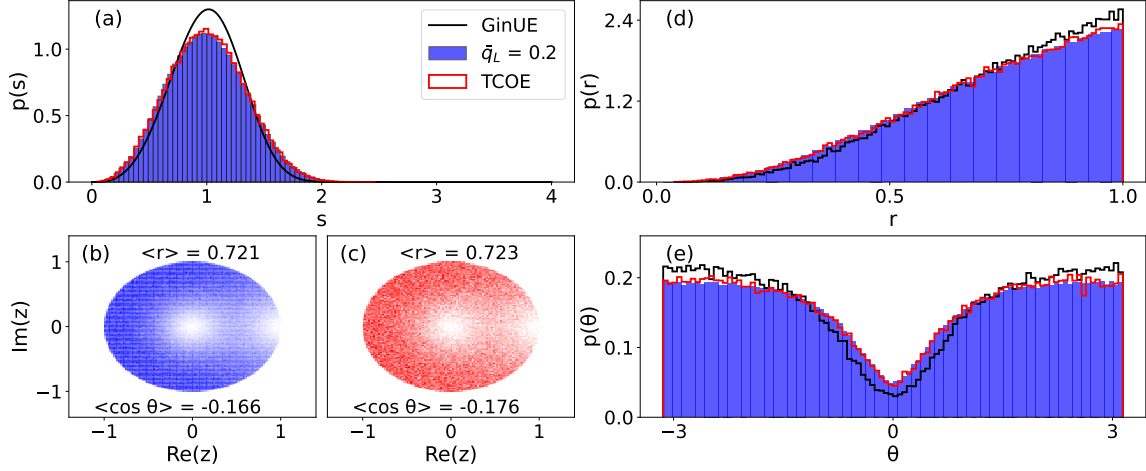


FIG. 5. Short-range spectral correlations for the leaky QSM with slit size and position $\Delta q = \bar{q}_L = 0.2$ (blue), compared with the TCOE (red) and the GinUE (black). (a) Nearest-neighbor eigenvalue spacing distributions for all three cases. (b)-(c) Distributions of ratios of consecutive eigenvalue spacings for (b) the leaky QSM and (c) the TCOE. The mean values $\langle r \rangle$ and $\langle \cos \theta \rangle$ are indicated. (d) Radius distribution of the ratio of consecutive spacings showing close agreement among the three ensembles. (e) Angle distribution of the ratio of consecutive spacings, demonstrating strong correspondence between the leaky QSM and the TCOE, and their deviation from the GinUE. Multiple ensemble realizations are used to ensure a total of at least 10^5 eigenvalues. The QSM ensemble is generated with $9.99 < K < 10.01$ and $N = 10^4$.

where $\Gamma(x, y)$ is the incomplete gamma function and the constant

$$C = \int_0^\infty s \tilde{p}(s) ds \approx 1.1429 \dots \quad (27)$$

ensures normalization and unit mean spacing, $\langle s \rangle = 1$.

While GinUE statistics are known to indeed capture universal spectral correlations in many open quantum chaotic systems, cases involving spatially localized openings have been less explored. Figure 5(a) compares the nearest-neighbor eigenvalue spacing distribution of the leaky QSM with $\Delta q = \bar{q}_L = 0.2$ (blue shade) to those of the TCOE (red curve) and the GinUE (black curve). The distribution for the QSM exhibits excellent agreement with the TCOE across the entire spectrum, even for small $|\lambda|$, where their density of states show discrepancies [see Fig. 4(a)]. However, both the leaky QSM and the TCOE deviate from the GinUE prediction.

The agreement observed in the nearest-neighbor spacing statistics between the leaky QSM (after excluding rapidly decaying resonances) and the TCOE, as shown in Fig. 5(a), reflects their similar spectral structure. Both spectra exhibit a pronounced accumulation of long-lived resonances near the unit circle, in contrast with the GinUE. In the leaky QSM, these long-lived resonances arise from classical trajectories that avoid the leak for many iterations, effectively sampling the phase space ergodically and developing chaotic correlations. This dynamical mechanism enables the associated quantum resonances to develop universal correlations consistent with the TCOE rather than Ginibre statistics.

2. Ratio of consecutive eigenvalue spacings

The ratio of consecutive eigenvalue spacings provides an alternative measure of short-range spectral correlations. Unlike spacing distributions, it does not require unfolding, which is useful in systems with nonuniform or difficult-to-model spectral densities. The complex ratio is defined as [9]

$$z_\mu = \frac{\lambda_\mu^{NN} - \lambda_\mu}{\lambda_\mu^{NNN} - \lambda_\mu}, \quad (28)$$

with λ_μ^{NN} (λ_μ^{NNN}) representing the nearest (next-nearest) neighbor of the eigenvalue λ_μ in the complex plane.

The ratio is typically expressed in the polar form $z_\mu = r_\mu e^{i\theta_\mu}$. For GinUE, the joint distribution $p(r, \theta)$ exhibits a characteristic annular (donut-like) structure, with an additional suppression of points along the real axis near $\theta = 0$ and $\theta = \pi$, producing a shape similar to “Pac-Man’s mouth”. The vanishing probability density at the origin reflects eigenvalue repulsion, a hallmark of chaotic non-Hermitian spectra. The reduced probability near $\theta = 0$ and $\theta = \pi$ arises from the tendency of the eigenvalues to avoid forming nearly collinear triplets [9]. A collinear triplet refers to three distinct eigenvalues whose positions in the complex plane lie approximately along the same straight line, so the spacing vectors from an eigenvalue to its nearest neighbor and to its second nearest neighbor have almost the same direction, leading to a very small angle, $\theta \approx 0$ and $\theta \approx \pi$.

The joint distributions $p(r, \theta)$ for the leaky QSM and the TCOE are shown in Fig. 5(b) and Fig. 5(c), respectively. Both display the characteristic Ginibre donut

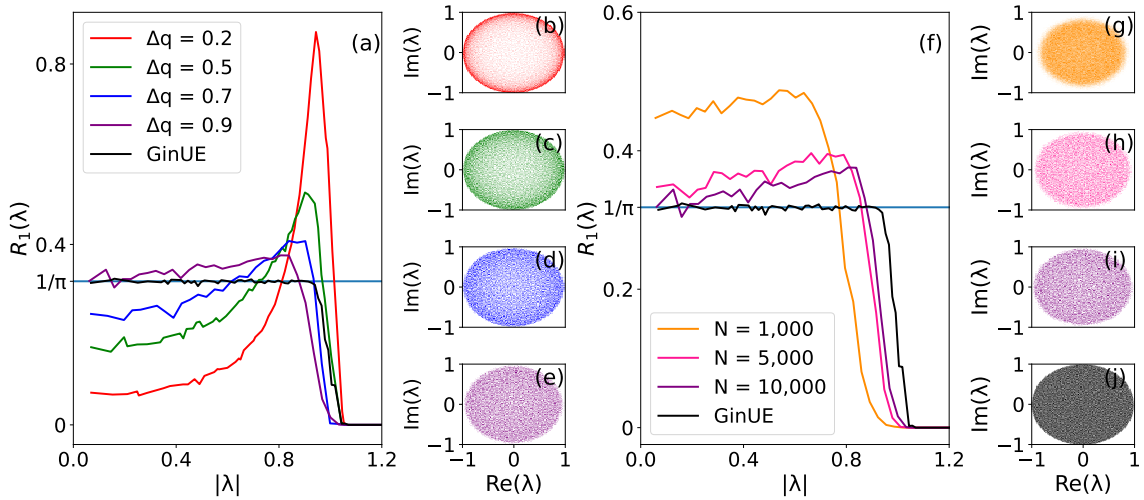


FIG. 6. Convergence of the density of states $R_1(\lambda)$ for the TCOE toward GinUE. (a) Averaged $R_1(\lambda)$ for TCOE with slit sizes $\Delta q = 0.2, 0.5, 0.7, 0.9$ (red, green, blue, and purple curve, respectively) compared with the numerical result for the GinUE (black line); $N = 10^4$. (b)-(e) Rescaled two-dimensional density states for the same slit sizes from (b) $\Delta q = 0.2$ to (e) $\Delta q = 0.9$, showing progressive homogenization of the spectrum as the leakage increases. (f) Averaged $R_1(\lambda)$ for TCOE with slit size $\Delta q = 0.9$ and dimensions $N = 1,000, 5 \times 10^3, 10^4$ (orange, pink, and purple curve, respectively) compared with the GinUE numerical result for $N = 10^4$ (black line). (g)-(i) Rescaled density of states for the TCOE with $N = 10^3, 5 \times 10^3, 10^4$ from (g) to (i) and for the GinUE in (j). Multiple ensemble realizations were considered to ensure at least 10^5 eigenvalues for each dataset.

shape, suggesting similar overall short-range correlations. However, the marginal distributions (probability distributions obtained by integrating either r or θ) reveal important differences, as discussed below. These projections are useful because they help to distinguish systems that look similar globally but differ in local symmetry or correlations. In particular, $p(r)$ characterizes the typical separation between neighboring eigenvalues and quantifies the strength of short-range level repulsion, while $p(\theta)$ reveals geometric correlations between nearby eigenvalues (as in the Ginibre's “gap” near the real axis) and exposes angular anisotropies.

In Fig. 5(d), the radial spacing distribution $p(r)$ for the leaky QSM (blue) and the TCOE (red) resemble that of the Ginibre ensemble (black). All three exhibit strong level repulsion, reflected in the vanishing probability density as $r \rightarrow 0$. Consistent with this behavior, the mean value of the spacing ratio, $\langle r \rangle$, for both the leaky QSM [Fig. 5(b)] and the TCOE [Fig. 5(c)] is close to the GinUE benchmark, $\langle r \rangle \approx 0.74$.

In contrast, Fig. 5(e) shows that the angular distribution $p(\theta)$ for the leaky QSM (blue) and the TCOE (red) deviate more noticeably from the GinUE prediction (black). In both cases, $p(\theta)$ is larger near $\theta \approx 0$ than for GinUE, indicating a higher probability of forming nearly collinear triplets than in the Ginibre case. This angular anisotropy reflects additional structure in the spectra of the leaky QSM and the TCOE that is absent in the isotropic GinUE. Consequently, their mean values $\langle \cos \theta \rangle$ differ from the GinUE benchmark of $\langle \cos \theta \rangle \approx -0.24$, confirming leak-induced modifications to the angular correlations.

We note that the angular distribution is especially sensitive to statistical fluctuations, requiring a large number of eigenvalues to obtain a smooth and reliable estimate. The results shown here are based on datasets containing at least 10^5 eigenvalues.

IV. LARGE LEAKAGE: GINIBRE VS. TRUNCATED CIRCULAR ENSEMBLE

As demonstrated in the preceding sections, the TCOE provides an effective random-matrix benchmark for the leaky QSM in the weak-to-moderate leakage regime, accurately capturing both its density of states and spectral correlations. A natural question is whether increasing the leakage size pushes the spectrum toward Ginibre universality. This question is motivated by the analytical results in Ref. [40], where it was shown that the properties of non-Hermitian matrices of size M , constructed as square submatrices of unitary random matrices of size N , converge to those of the Ginibre ensemble as the ratio M/N becomes sufficiently small.

Because the number of surviving resonances decreases dramatically at large leakage (e.g., only 0.01% of resonances remain at $\Delta q = 0.9$), direct analysis of the leaky QSM becomes computationally prohibitive. In this strongly open regime, the TCOE provides a tractable surrogate for the leaky QSM.

In Fig. 6, we examine how the density of states and spectral correlations of the TCOE change as the leakage increases and compare them with the GinUE. The density of states and the distribution of eigenvalues in the

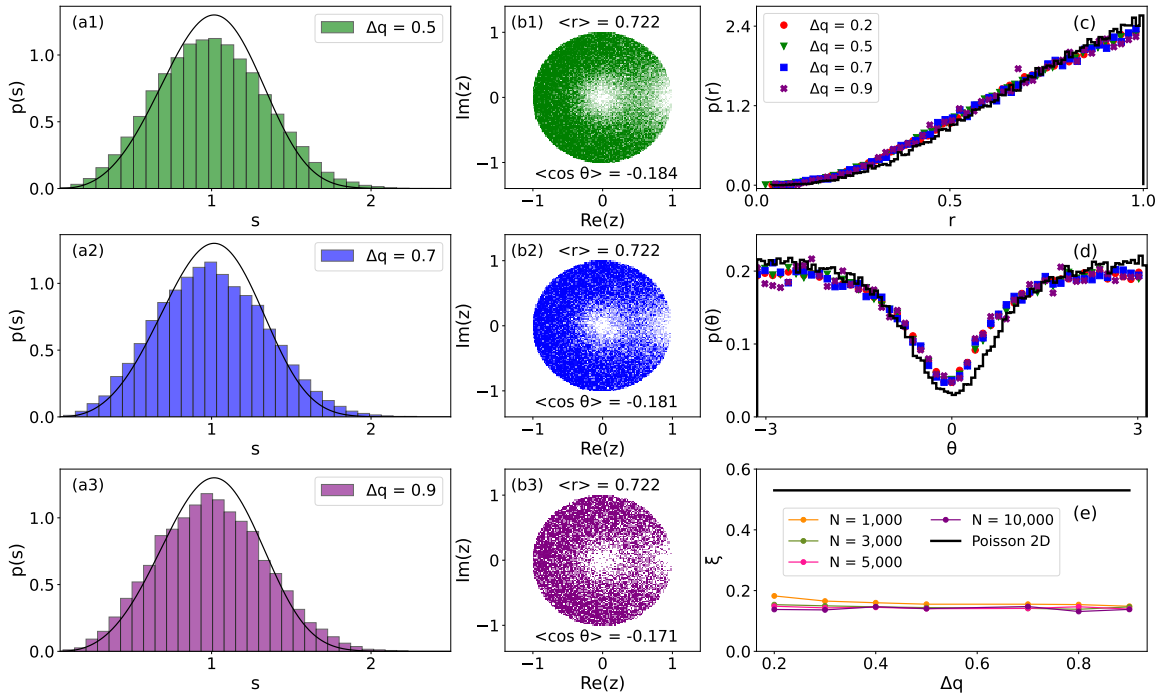


FIG. 7. Short-range spectral correlations of the TCOE compared with the GinUE. (a1)-(a3) Nearest-neighbor spacing distributions for TCOE with slit sizes $\Delta q = 0.5, 0.7, 0.9$ (green, blue, and purple shades) alongside the GinUE distribution (black line). No convergence toward GinUE statistics is observed as the truncation increases. (b1)-(b3) Distributions of the ratio of consecutive spacings for the same slit sizes from (b1) $\Delta q = 0.5$ to (b3) $\Delta q = 0.9$. The mean values of radius $\langle r \rangle$ and angular indicator $\langle \cos \theta \rangle$ are shown. (c) Radius distribution of the ratio of consecutive spacings, showing close agreement across all TCOE cases and with GinUE. (d) Angle distribution of the ratio of consecutive spacings, highlighting the consistency among TCOE ensembles and their persistent deviation from GinUE predictions. In all panels, except (e), $N = 10^4$. (e) Scaling analysis of the deviation between TCOE and GinUE nearest-neighbor spacing statistics, quantified with the level spacing indicator (LSI) [see Eq. (29)], shown as function of the slit size for matrix dimensions $N = 10^3, 3 \times 10^3, 5 \times 10^3, 10^4$ (orange, olive, pink, and purple curves). For reference, the LSI of the 2D Poisson ensemble associated with integrable systems is included. Multiple ensembles are considered to ensure at least 10^5 eigenvalues per dataset.

complex plane characterize global statistical properties, while spacing and ratio distributions probe local spectral correlations. These measures are therefore complementary. Our results reveal a dichotomy. Although the density of states gradually converges toward the Ginibre prediction as the leakage grows, the local spectral correlations remain distinct from GinUE statistics even in the limit of very large truncation.

Figure 6(a) shows how the smoothed density of states of the TCOE converges to the GinUE prediction as the slit width Δq increases. For moderate leakage ($\Delta q = 0.2$, red line), long-lived resonances persist and accumulate near the unit circle [Fig. 6(b)], so $R_1(\lambda)$ strongly deviates from the GinUE uniform $1/\pi$ profile. As the leak grows ($\Delta q = 0.5, 0.7$, and 0.9 ; green, blue, and purple curves), the distribution undergoes a qualitative transition: The accumulation near $|\lambda| \approx 1$ gradually disappears [cf. Figs. 6(b)-(e)], and the distribution becomes increasingly uniform, approaching the Ginibre limit. This trend is consistent with earlier predictions from non-unitary random matrix theory in [36, 37, 40]. The convergence is further enhanced with increasing matrix dimension, as

illustrated in Fig. 6(f) for $\Delta q = 0.9$.

In contrast, the spectral-correlation analysis in Fig. 7 reveals a different behavior. Despite the TCOE density of states converging toward Ginibre statistics as the leakage increases, the local correlations do not approach those of the GinUE.

Figures 7(a1)-(a3) show that the nearest-neighbor spacing distributions for the TCOE with $\Delta q = 0.5, 0.7, 0.9$ (green, blue, and purple) remain essentially unchanged across slit sizes. The distributions closely match the one for the moderate-leak case in Fig. 5(a) for $\Delta q = 0.2$ and do not converge toward the GinUE result (black line).

The disagreement with the GinUE is further supported by the mean values of the spacing-ratio indicators displayed alongside the ratio distributions for the same slit sizes in Figs. 7(b1)-(b3). These values remain consistent with those reported in Fig. 5(c). Across all slit sizes, the mean radius remains approximately $\langle r \rangle \sim 0.72$, close to the GinUE benchmark $\langle r \rangle_{\text{GinUE}} \approx 0.74$, while the angular indicator stays noticeably different, with $|\langle \cos \theta \rangle| < 0.19$ deviating from the GinUE value

$|\langle \cos \theta \rangle_{\text{GinUE}}| \approx 0.24$. Furthermore, considering also the values in Fig. 5(c), neither quantity exhibits a systematic trend with increasing leakage; instead, both fluctuate as the leak size grows, indicating no approach toward Ginibre statistics.

Figures 7(c)-(d) present results for four slit sizes, $\Delta q = 0.2, 0.5, 0.7, 0.9$, which are consistent with the discussion above. The radius distributions in Fig. 7(c) agree closely across all TCOE cases and are similar to the GinUE prediction. In contrast, the angular distributions in Fig. 7(d) continue to deviate from the Ginibre expectations even at the largest leakage ($\Delta q = 0.9$).

In Fig. 7(e), we quantify the deviation of the nearest-neighbor spacing distribution $p(s)$ for the TCOE from the analytical results for GinUE using the level spacing indicator,

$$\xi = \frac{\sum_i |p(s_i) - p_{\text{GinUE}}(s_i)|}{\sum_i p_{\text{GinUE}}(s_i)}. \quad (29)$$

The figure shows ξ as a function of the leak size for different matrix dimensions. For comparison, the value corresponding to the 2D Poisson ensemble, representative of integrable systems, is also included (black line). The ξ curves are nearly flat, displaying no systematic dependence on Δq , and they lie almost on top of one another for all matrix sizes. This indicates that, for the parameters considered, increasing either the truncation strength or the system size does not lead to convergence toward GinUE statistics.

The persistence of TCOE spectral characteristics across all leakage strengths shows that increasing openness does not wash out correlations intrinsic to truncated ensembles. Instead, their spectral correlations remain stable, even when the density of states approaches the Ginibre limit. This robustness suggests that truncated random matrices form a distinct universality class for open quantum systems, fundamentally different from the GinUE, despite exhibiting similar global statistics at strong truncation.

V. CONCLUSIONS

We investigated the spectral properties of the leaky quantum standard map (QSM), which is an open Floquet system with a strongly chaotic classical limit and a spatially localized leak, and compared its spectral properties with those of the truncated circular orthogonal ensemble (TCOE) and the Ginibre unitary ensemble (GinUE). Our results demonstrate that the commonly assumed Ginibre

universality for open quantum-chaotic systems does not generally apply when the openness is spatially localized.

For the long-lived resonances, which correspond to classical trajectories that avoid the leak for many iterations and therefore explore the phase space in an approximately ergodic manner, we find quantitative agreement with the TCOE in both the density of states and the short-range spectral correlations. This agreement persists for a wide range of moderate leak sizes. In contrast, these same resonances systematically deviate from GinUE predictions, exhibiting a pronounced accumulation near the unit circle and spectral correlations distinct from the Ginibre statistics.

Short-lived resonances behave differently. They form a nonuniversal cluster near the origin of the complex plane and do not follow either TCOE or GinUE statistics. Their structure reflects the underlying non-ergodic Floquet eigenstates localized near the leak in the closed system, and thus encodes system-specific features.

Motivated by earlier studies that sufficiently strong truncation could take random matrices toward the Ginibre limit, we also analyzed the TCOE as the truncation ratio increases. While the density of states of the TCOE indeed approaches the GinUE circular law, the spectral correlations do not converge to the Ginibre prediction. This suggests that truncated unitary ensembles form a separate non-Hermitian universality class.

Taken together, our results show that the spectral statistics of long-lived resonances in quantum-chaotic systems with localized leakage are accurately captured by the TCOE rather than by the GinUE. This insight clarifies the limits of Ginibre universality in open quantum systems and has direct relevance for interpreting experiments in microwave and optical billiards, quantum dots, and other platforms where loss is spatially localized. Interesting future directions include exploring multiple leaks and time-dependent openness.

ACKNOWLEDGMENTS

This research was supported by the Research Corporation Cottrell SEED award CS-SEED-2025-003.

VI. CODE AND DATA AVAILABILITY

All the codes and data used to generate the figures in the manuscript analysis and dynamical simulations can be found at <https://github.com/edsonsignor/QSM-leakage>.

[1] E. P. Wigner, On the statistical distribution of the widths and spacings of nuclear resonance levels, Proc. Cambridge Phil. Soc. **47**, 790 (1951).

[2] F. J. Dyson, The threefold way. algebraic structure of symmetry groups and ensembles in quantum mechanics, J. Math. Phys. **3**, 1199 (1962).

- [3] M. L. Mehta, *Random Matrices* (Academic Press, Boston, 1991).
- [4] F. Haake, *Quantum Signatures of Chaos* (Springer-Verlag, Berlin, 1991).
- [5] T. Guhr, A. Müller-Groeling, and H. A. Weidenmüller, Random matrix theories in quantum physics: Common concepts, *Phys. Rep.* **299**, 189 (1998).
- [6] R. Grobe, F. Haake, and H.-J. Sommers, Quantum distinction of regular and chaotic dissipative motion, *Phys. Rev. Lett.* **61**, 1899 (1988).
- [7] R. Grobe and F. Haake, Universality of cubic-level repulsion for dissipative quantum chaos, *Phys. Rev. Lett.* **62**, 2893 (1989).
- [8] G. Akemann, M. Kieburg, A. Mielke, and T. Prosen, Universal signature from integrability to chaos in dissipative open quantum systems, *Phys. Rev. Lett.* **123**, 254101 (2019).
- [9] L. Sá, P. Ribeiro, and T. Prosen, Complex spacing ratios: A signature of dissipative quantum chaos, *Phys. Rev. X* **10**, 021019 (2020).
- [10] R. Hamazaki, K. Kawabata, N. Kura, and M. Ueda, Universality classes of non-Hermitian random matrices, *Phys. Rev. Res.* **2**, 023286 (2020).
- [11] S. Denisov, T. Laptysheva, W. Tarnowski, D. Chruściński, and K. Życzkowski, Universal spectra of random Lindblad operators, *Phys. Rev. Lett.* **123**, 140403 (2019).
- [12] L. Sá, P. Ribeiro, and T. Prosen, Spectral and steady-state properties of random Liouvillians, *J. Phys. A* **53**, 305303 (2020).
- [13] Álvaro Rubio-García, R. A. Molina, and J. Dukelsky, From integrability to chaos in quantum Liouvillians, *SciPost Phys. Core* **5**, 026 (2022).
- [14] A. M. García-García, L. Sá, and J. J. M. Verbaarschot, Symmetry classification and universality in non-Hermitian many-body quantum chaos by the Sachdev-Ye-Kitaev model, *Phys. Rev. X* **12**, 021040 (2022).
- [15] K. Kawabata, A. Kulkarni, J. Li, T. Numasawa, and S. Ryu, Symmetry of open quantum systems: Classification of dissipative quantum chaos, *PRX Quantum* **4**, 030328 (2023).
- [16] M. Prasad, H. K. Yadalam, C. Aron, and M. Kulkarni, Dissipative quantum dynamics, phase transitions, and non-Hermitian random matrices, *Phys. Rev. A* **105**, L050201 (2022).
- [17] K. Wold, Z. Zhu, F. Jin, X. Zhu, Z. Bao, J. Zhong, F. Shen, P. Zhang, H. Li, Z. Wang, C. Song, Q. Guo, S. Denisov, L. Sá, H. Wang, and P. Ribeiro, Experimental detection of dissipative quantum chaos (2025), arXiv:2506.04325 [quant-ph].
- [18] T. Prosen and T. H. Seligman, Quantization over boson operator spaces, *J. Phys. A* **43**, 392004 (2010).
- [19] T. Can, V. Oganesyan, D. Orgad, and S. Gopalakrishnan, Spectral gaps and midgap states in random quantum master equations, *Phys. Rev. Lett.* **123**, 234103 (2019).
- [20] I. Vallejo-Fabila, A. K. Das, D. A. Zarate-Herrada, A. S. Matsoukas-Roubeas, E. J. Torres-Herrera, and L. F. Santos, Reducing dynamical fluctuations and enforcing self-averaging by opening many-body quantum systems, *Phys. Rev. B* **110**, 075138 (2024).
- [21] D. Villaseñor and P. Barberis-Blostein, Analysis of chaos and regularity in the open Dicke model, *Phys. Rev. E* **109**, 014206 (2024).
- [22] F. Roccati, F. Balducci, R. Shir, and A. Chenu, Diagnosing non-Hermitian many-body localization and quantum chaos via singular value decomposition, *Phys. Rev. B* **109**, L140201 (2024).
- [23] D. C. Brody, Biorthogonal quantum mechanics, *J. Phys. A* **47**, 035305 (2013).
- [24] G. De Tomasi and I. M. Khaymovich, Non-Hermitian Rosenzweig-Porter random-matrix ensemble: Obstruction to the fractal phase, *Phys. Rev. B* **106**, 094204 (2022).
- [25] J. Máč, M. J. Bhaseen, and G. Pal, Arijeet, Statics and dynamics of non-Hermitian many-body localization, *Commun. Phys.* **7**, 1 (2024).
- [26] J. Ginibre, Statistical ensembles of complex, quaternion, and real matrices, *J. Math. Phys.* **6**, 440 (1965).
- [27] Y. V. Fyodorov, B. A. Khoruzhenko, and H.-J. Sommers, Almost Hermitian random matrices: Crossover from Wigner-Dyson to Ginibre eigenvalue statistics, *Phys. Rev. Lett.* **79**, 557 (1997).
- [28] Y. V. Fyodorov and H.-J. Sommers, Random matrices close to Hermitian or unitary: overview of methods and results, *J. Phys. A* **36**, 3303 (2003).
- [29] D. Villaseñor, L. F. Santos, and P. Barberis-Blostein, Breakdown of the quantum distinction of regular and chaotic classical dynamics in dissipative systems, *Phys. Rev. Lett.* **133**, 240404 (2024).
- [30] D. Mondal, A. Kolovsky, and S. Sinha, Dissipative chaos and steady state of an open Tavis-Cummings dimer, *Phys. Rev. E* **111**, L052204 (2025).
- [31] D. Mondal, L. F. Santos, and S. Sinha, Transient and steady-state chaos in dissipative quantum systems (2025), arXiv:2506.05475 [quant-ph].
- [32] F. Ferrari, L. Gravina, D. Eeltink, P. Scarlino, V. Savona, and F. Minganti, Dissipative quantum chaos unveiled by stochastic quantum trajectories, *Phys. Rev. Res.* **7**, 013276 (2025).
- [33] D. Bernard and A. LeClair, A classification of non-hermitian random matrices, in *Statistical Field Theories* (Springer Netherlands, Dordrecht, 2002) pp. 207–214.
- [34] E. G. Altmann, J. S. E. Portela, and T. Tél, Leaking chaotic systems, *Rev. Mod. Phys.* **85**, 869 (2013).
- [35] K. Holmes, J. Hall, and E.-M. Graefe, Intensity landscapes in elliptic and oval billiards with a circular absorbing region, *Phys. Rev. E* **112**, 034202 (2025).
- [36] Y. V. Fyodorov and H.-J. Sommers, Statistics of resonance poles, phase shifts and time delays in quantum chaotic scattering: Random matrix approach for systems with broken time-reversal invariance, *J. Math. Phys.* **38**, 1918 (1997).
- [37] Y. V. Fyodorov and B. A. Khoruzhenko, Systematic analytical approach to correlation functions of resonances in quantum chaotic scattering, *Phys. Rev. Lett.* **83**, 65 (1999).
- [38] G. Casati, B. V. Chirikov, F. M. Izrailev, and J. Ford, Stochastic behavior of a quantum pendulum under a periodic perturbation, *Lect. Notes in Phys.* **9399**, 334 (1979).
- [39] M. Novaes, Resonances in open quantum maps, *J. Phys. A* **46**, 143001 (2013).
- [40] K. Życzkowski and H.-J. Sommers, Truncations of random unitary matrices, *J. Phys. A* **33**, 2045 (2000).
- [41] M. Glück, A. R. Kolovsky, and H. J. Korsch, Lifetime statistics for a bloch particle in ac and dc fields, *Phys. Rev. E* **60**, 247 (1999).

- [42] R. Killip and R. Kozhan, Matrix models and eigenvalue statistics for truncations of classical ensembles of random unitary matrices, *Commun. Math. Phys.* **349**, 9911027 (2017).
- [43] J. Fischmann, W. Bruzda, B. A. Khoruzhenko, H.-J. Sommers, and K. Życzkowski, Induced Ginibre ensemble of random matrices and quantum operations, *J. Phys. A* **45**, 075203 (2012).
- [44] H. Schomerus and J. Tworzydlo, Quantum-to-classical crossover of quasibound states in open quantum systems, *Phys. Rev. Lett.* **93**, 154102 (2004).
- [45] D. L. Shepelyansky, Fractal Weyl law for quantum fractal eigenstates, *Phys. Rev. E* **77**, 015202 (2008).
- [46] B. V. Chirikov, Research concerning the theory of non-linear resonance and stochasticity, *CERN-Trans* , 7140 (1971).
- [47] L. E. Reichl, *The Transition to Chaos: Conservative Classical Systems and Quantum Manifestations*, 2nd ed. (Springer, 2004).
- [48] The effective \hbar incorporates the physical scales of the rotor (period and moment of inertia), which are set to unity in our dimensionless formulation of the standard map in Eq. (2).
- [49] M. Berry, N. Balazs, M. Tabor, and A. Voros, Quantum maps, *Ann. Phys.* **122**, 26 (1979).
- [50] A. Lakshminarayanan, Classical and quantum chaos plus RMT and some applications, Lecture notes for the Bangalore Summer School on Statistical Physics (2018).
- [51] K. Husimi, Some formal properties of the density matrix, *J. Phys. Soc. Jpn.* **22**, 264 (1940).
- [52] K. Zyczkowski, Quantum chaotic system in the generalized husimi representation, *Phys. Rev. A* **35**, 3546 (1987).
- [53] M. Saraceno, Classical structures in the quantized baker transformation, *Ann. Phys.* **199**, 37 (1990).
- [54] A. Bäcker, Numerical aspects of eigenvalue and eigenfunction computations for chaotic quantum systems, in *The Mathematical Aspects of Quantum Maps* (Springer Berlin Heidelberg, 2003) pp. 91–144.
- [55] J. Hall, S. Malzard, and E.-M. Graefe, Semiclassical Husimi distributions of Schur vectors in non-Hermitian quantum systems, *Phys. Rev. Lett.* **131**, 040402 (2023).
- [56] M. A. P. Reynoso, E. M. Signor, S. D. Prado, and L. F. Santos, Effects of stickiness on the quantum states of strongly chaotic open systems, *Phys. Rev. E* **110**, L062201 (2024).
- [57] B. A. Khoruzhenko and H. J. Sommers, Non-hermitian random matrix ensembles (2009), arXiv:0911.5645 [math-ph].
- [58] J. M. Pedrosa, G. G. Carlo, D. A. Wisniacki, and L. Ermann, Distribution of resonances in the quantum open baker map, *Phys. Rev. E* **79**, 016215 (2009).
- [59] S. Nonnenmacher and M. Zworski, Distribution of resonances for open quantum maps, *J. High Energ. Phys.* **269**, 311.
- [60] S. Mudute-Ndumbe and E.-M. Graefe, A non-Hermitian PT-symmetric kicked top, *NJP* **22**, 103011 (2020).
- [61] C. Jisha and R. Prakash, Universality of spectral fluctuations in open quantum chaotic systems, *EPL* **146**, 11001 (2024).
- [62] F. Haake, F. Izrailev, N. Lehmann, D. Saher, and H.-J. Sommers, Statistics of complex levels of random matrices for decaying systems, *Z. Phys. B* **88**, 359370 (1992).
- [63] This method is equivalent to that used for Hermitian matrices described in [64], where each subset of k consecutive level spacings, s_{i+1}, \dots, s_{i+k} , are divided by the local mean spacing given by $(E_{i+k+1} - E_{i+1})/k$. We usually choose $1 \ll k \lesssim 10$.
- [64] A. Gubin and L. F. Santos, Quantum chaos: An introduction via chains of interacting spins 1/2, *Am. J. Phys.* **80**, 246 (2012).